STRUCTURAL PROPERTIES OF A SOL-GEL GENERATED $BiFeO_3$ AND ITS PHOTOCATALYTIC ACTIVITY

Truong Thi Thao[1], Nguyen Anh Vu[2], Chu Thi Anh Xuan[1], Lo Thi Hue[1], Nguyen Thi Khanh Van[1], Le Tien Ha[1], Nguyen Van Khien[1*]
[1]TNU - University of Science, [2]Hanoi University of Pharmacy

ARTICLE INFO

Received: 04/01/2024
Revised: 25/3//2024
Published: 25/3//2024

KEYWORDS

$BiFeO_3$
Sol-gel
Photocatalysis
Bandgap
Methylene Blue

ABSTRACT

$BiFeO_3$ (BFO) was synthesized using a combustion sol-gel method from reactants of $Bi(NO_3)_3.5H_2O$ and $Fe(NO_3)_3.9H_2O$ with various complexation reagents. The XRD results indicated that the synthesized BFO materials, which were obtained by using a complexation reagent of tartaric acid and annealed at 600 ºC or 700 ºC in two hours, have a single phase of orthorhombic perovskite structure, belongs to R3c symmetry group. The absorbance and photocatalytic activity of BFO on Methylene Blue (MB) decomposition were studied using infrared (IR) and UV-Vis spectroscopy. With a hollow porous morphology and a narrow bandgap of ~2.20 eV, our obtained bulk BFO material almost does not absorb but become a solar photocatalyst for degradation of MB. Using BFO at 1.0 g/L, the degradation of MB can reach 90% after 90 minutes of illumination with MB concentrations of 10 - 30 ppm. This was confirmed that photoexcited e-h pairs are responsible for the degradation of MB under sunlight.

NGHIÊN CỨU CẤU TRÚC VÀ KHẢ NĂNG QUANG XÚC TÁC CỦA $BiFeO_3$ ĐƯỢC CHẾ TẠO BẰNG PHƯƠNG PHÁP SOL-GEL

Trương Thị Thảo[1], Nguyễn Anh Vũ[2], Chu Thị Anh Xuân[1], Lô Thị Huế[1], Nguyễn Thị Khánh Vân[1], Lê Tiến Hà[1], Nguyễn Văn Khiển[1*]
[1]Trường Đại học Khoa học - ĐH Thái Nguyên, [2]Trường Đại học Dược Hà Nội

THÔNG TIN BÀI BÁO

Ngày nhận bài: 04/01/2024
Ngày hoàn thiện: 25/3//2024
Ngày đăng: 25/3//2024

TỪ KHÓA

$BiFeO_3$
Sol-gel
Xúc tác quang
Năng lượng vùng cấm
Xanh Methylene

TÓM TẮT

$BiFeO_3$ (BFO) được chế tạo bằng phương pháp sol-gel từ các tiền chất ban đầu $Bi(NO_3)_3.5H_2O$ và $Fe(NO_3)_3.9H_2O$. Kết quả phân tích giản đồ nhiễu xạ tia X cho thấy hệ vật liệu BFO chế tạo được khi nung ở 600 ^oC và 700 ^oC là đơn pha với cấu trúc Provskie trực giao, thuộc nhóm đối xứng không gian R3c. Độ hấp thụ và hoạt tính quang xúc tác của BFO đối với quá trình phân hủy xanh Methylene (MB) được nghiên cứu bằng phương pháp quang phổ hồng ngoại (IR) và UV-Vis. Qua tính toán BFO có độ rộng vùng cấm khoảng 2,20 eV và gần như không hấp thụ MB nhưng nó lại có khả năng làm chất xúc tác quang phân huỷ MB rất tốt dưới ánh sáng mặt trời. Ứng với nồng độ 1,0 g/L của BFO nó có khả năng phân hủy MB ở nồng độ MB từ 10 - 30 ppm đạt tới 90% sau 90 phút chiếu sáng. Điều này chứng minh rằng các cặp điện tử - lỗ trống (e-h) bị kích thích quang là nguyên nhân gây ra sự phân hủy MB dưới ánh sáng mặt trời.

DOI: https://doi.org/10.34238/tnu-jst.9542

* Corresponding author. *Email: khiennv@tnus.edu.vn*

1. Introduction

Nowadays, $BiFeO_3$ (BFO) material has been extensively studied for its interesting properties, such as the coexistence of ferroelectric phase and antiferromagnetic phase, adjustable band-gap energy (E_g) (E_g ~ 1.3 – 3.1 eV depending on its structure, shape and size) [1] – [6]. These characteristics make BFO a highly hopeful material, particularly in photocatalysis. However, the crystal structure and physical characteristics of BFO are heavily influenced by fabrication techniques. Many studies have been conducted to concentrate on the fabrication of BFO using various techniques in order to produce single-phase BFO, but few have been successful [3], [7], [8]. One of the most commonly described techniques is solid state reaction [9], [10], which can be more easily manufactured as a single phase. However, materials made using this technique almost always need to be sintered at high temperatures, and the resulting particles are typically large (μm), resulting in poorer photocatalytic effectiveness due to lower surface area. Other chemical methods such as hydrothermal [11], [12], sol-gel [13], and coprecipitate [14], [15] have been used to employ BFO nanoparticles (NPs) and related nanopowders with well-crystalline, nano-size, and no secondary phases, which are thought to be advantageous for photocatalytic applications. Sol-gel synthesis of nanoparticles is one of them, and the simplicity of the method for producing functional oxides has piqued the attention of many academics. This is because the technique is convenient and flexible, produces pure powders, and can be used to create materials with excellent surface area, size, and morphology control [16]. Furthermore, when compared to the other methods, the sol-gel technique demonstrated some benefits in regulating the chemical composition and size of BFO NPs. For instance, previous works have shown that the BFO NPs produced by the sol-gel technique could be used as a photocatalyst for various dyes such as Methyl orange (MO) [17] – [19], Rhodamine B (RhB) [20], [21], and Methylene Blue (MB) [22]. Therefore, in this study, we focused on the fabrication of high quality BFO NPs using sol-gel method, for application in photocatalysts.

2. Experiment

BFO NPs were synthesized using a sol-gel technique with $Bi(NO_3)_3.5H_2O$ and $Fe(NO_3)_3.9H_2O$ predecessors. As complexation reagents, tartaric acid and polyvinyl were used. The obtained gels were then annealed at different temperatures from 400 ºC to 700 ºC in 2 h. The crystalline structure of NPs was investigated using an X-ray diffractometer. The surface morphology of samples was examined using a scanning electron microscope (SEM). The optical properties of BFO NPs were investigated using infrared (IR) spectroscopy and UV-vis spectrometer. The photocatalytic activity of BFO was tested by degrading MB under the influence of sunlight. In various pH environments of 3, 7, and 11, the MB was dissolved to varied concentrations of 10, 20, and 30 ppm, which were adjusted using NaOH and HCl. The BFO NPs were stirred into the MB solution in increments of 0.5, 1.0, and 1.5 g/L. By resting BFO in MB solution for 10 - 90 minutes, the adsorption of MB to BFO was evaluated. The MB solution was centrifuged after settling to remove BFO NPs. The leftover quantity of MB was then evaluated using UV-Vis absorbance, which allows the adsorbed and degraded amount of MB to be calculated.

3. Results and discussions

3.1. Characterization of BFO

Figure 1 depicted the development of the crystalline structure of BFO samples as the heating temperature is increased (T_A). It is demonstrated that the formation of BFO phase was highly influenced by the T_A. At low T_A, beside the diffraction peak of BFO, there were several diffraction peaks of other unknown phases, suggesting the uncompleted formation of BFO. The peak intensities of these secondary phases dropped as T_A increased. These peaks almost disappeared under T_A of 550 ºC, except a peak located at $2\theta = 28$ º of $Bi_{25}FeO_{40}$. At T_A of 600 ºC,

formation of BFO was completed, without any secondary phase. All of the diffraction peaks belong to orthorhombic perovskite BFO, corresponding to (012), (104), (110), (006), (202), (024), (116), (122), (018) and (214) plane. These peaks matched very well with JPCDS 01-071 – 2494 card of BFO (ICDD database) [23]. According to this database, BFO has structure of deformation orthorhombic perovskite structure, which belongs to symmetry group R3c with lattice constants a = b = 5,587 Å and c = 13,867 Å, with diffraction peak intensity ratio of $I_{(104)}/I_{(100)}$ ~1. XRD results reveal that single- phase BFO material has been successfully synthesized from the reaction of nitrates of Bi and Fe with complexation reagent of tartaric acid and annealing temperature higher than 600 ºC.

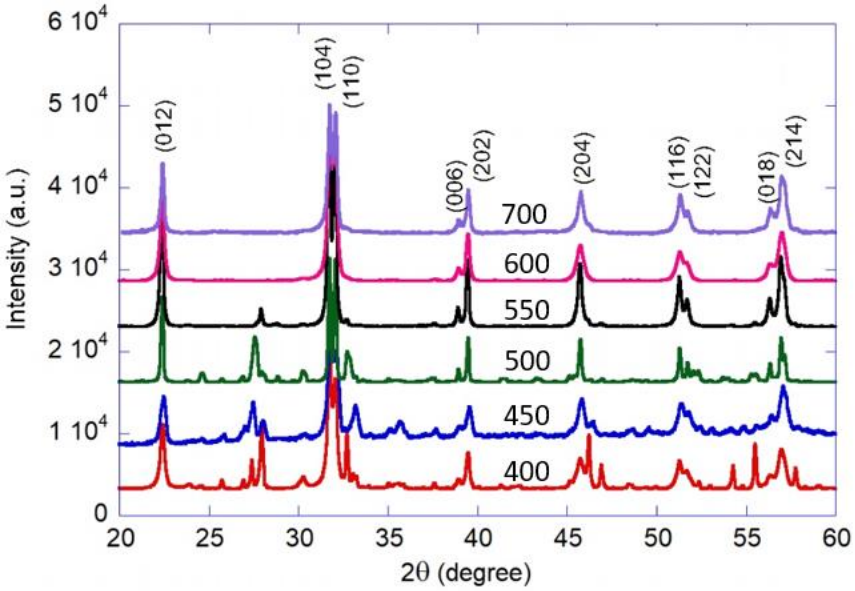

Figure 1. *XRD profiles of BFO synthesized at different annealing temperatures*

Morphology, size and shape of BFO particles, which were annealed at 600 ºC and 700 ºC, were investigated using SEM (Figure 2). At T_A of 600 ºC, it was hard to see the boundaries between BFO particles. The particles stick together to form a porous hollow structure as a honeycomb. This structure allows high BET surface area, which is requisite for catalysts, catalyst delivery agent, or adsorbents. At higher temperature, T_A of 700 ºC, the hollow structure no longer exists. BFO transforms to the form of dense particles, varying from 50 to 100 nm in size.

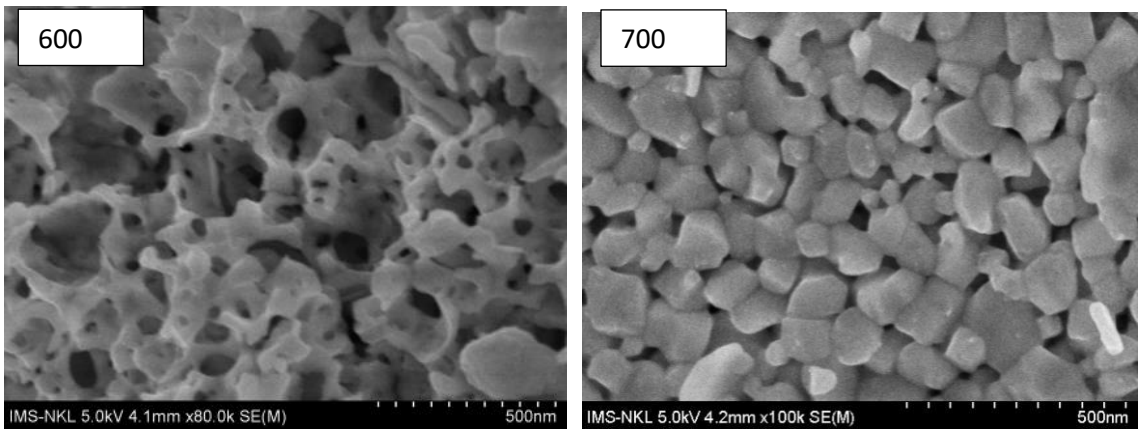

Figure 2. *SEM images of $BiFeO_3$ samples*

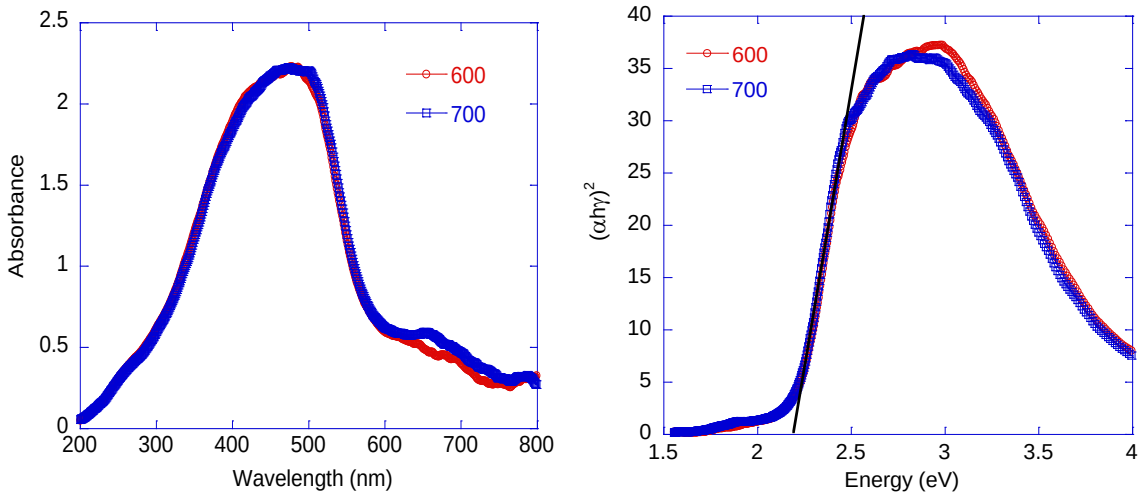

Figure 3. *Absorbance spectra and Tauc plot of BFO powders annealed at 600 °C and 700 °C*

Narrow band gap energy is one critical factor for the applicability in solar photocatalysts. Band gap energies of BFO powders annealed at 600 and 700 ºC were calculated via absorption spectra, which were investigated using solid UV-Vis spectroscopy (Figure 3) with Kubelka-Munk theory [24]. As shown in Figure 3(a), BFO powders have noticeably wide absorption range. BFO powders do not have sharp absorption edges but are quite broad, due to variation in the crystalline size according to SEM images. The photo absorbance of BFO powders reaches the maximum at ~ 450 nm. The Tauc plot (Figure 3 b) shows two edges of absorption. The main absorption edge is located at 2.2 eV, which is direct band-to-band absorption. This obtained value of the band gap of BFO NPs was similar results of previous works, which ranged from 19.7 to 2.32 eV [17] – [22]. This absorption most probably is attributed to the absorption of electrons from O *2p* level in valence band to Fe 3*d* in conduction band. Another absorption edge located at energy of ~1.6 eV, is revealed by an absorption tail in absorbance spectra. This tail can be explained by the absorption of electron from energy level T_2g to the E_g level of d-orbital of Fe ion [25]. This absorption is of course much lower than the previous one. Noticeably, there was not much difference between absorption of samples annealed at 600 ºC and 700 ºC, except small difference in the absorption tail in the range of 600-800 nm. These results confirm that with T_A no less than 600 ºC, obtained BFO powders are single phases and then, their band gap energy does not depend on the T_A.

3.2. Photocatalytic activity study

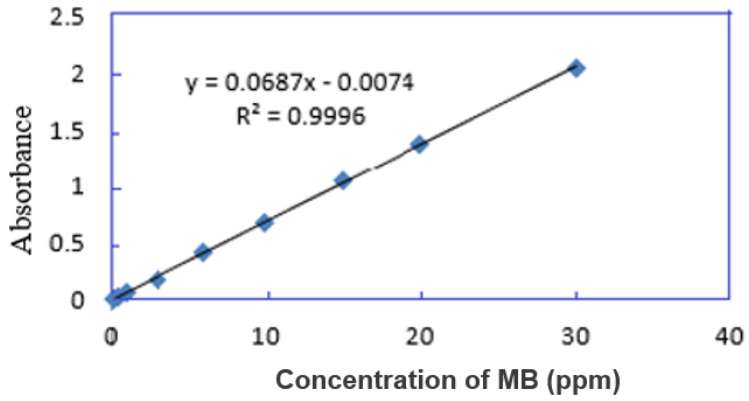

Figure 4. *Evolution of absorbance at 664 nm of a reference MB solution with MB concentration*

Concentration of MB in aqueous solution was determined by the absorbance at 664 nm measured using UV-Vis spectrometer for 480-720 nm range. Evolution of the absorbance of a reference MB solution at 664 nm with MB concentration was presented in Figure 4. For the MB concentration in the range of 0.1 – 30 ppm, the absorbance was linearly proportional to the concentration of MB in the solution. This linear relation allows us to use this method to evaluate the photocatalytic effect via the properly determination of the concentration of MB using absorbance at 664 nm.

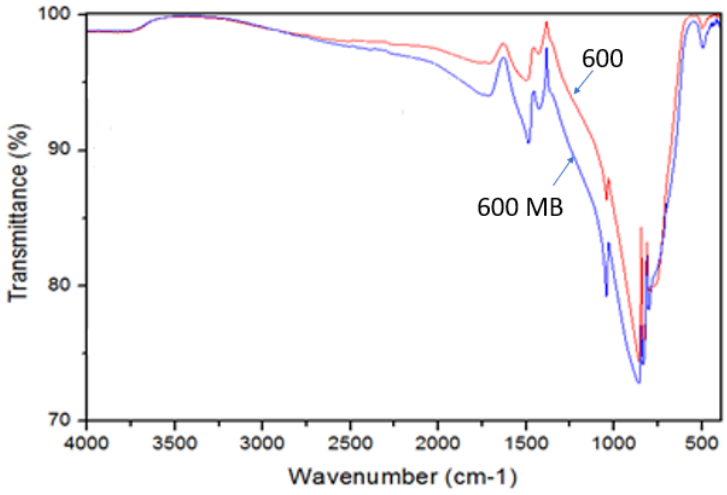

Figure 5. *600^{o}C infrared spectrum before and after the adsorption of MB*

Figure 5 shows the IR spectra of BFO samples, annealed at 600 and 600 MB, before and after MB adsorption. It can be seen that both 600 and 600 MB samples showed the absorption peaks in the range of 400 – 600 cm^{-1}. These peaks can be attributed to the stretching vibration mode and bending vibration mode of O-Fe bonds in the octahedral FeO_6 in perovskite [12]. Besides, there are absorption peaks located at 794 cm^{-1}, 827 cm^{-1}, and 852 cm^{-1} which are characteristic peaks of the vibration of metal-oxy bonds (Bi-O; Fe-O) in the phase R3c of BFO [26]. Another absorption peak located at 1041 cm^{-1} also involves in vibration of Bi-O bonds. These results confirm the formation of single phase BFO under annealing at 600 ºC.

Table 1. *Adsorbance of MB onto BFO 700^{o}C after 60 min in dark*

BFO 700^{o}C concentration (g/L)	MB concentration (ppm)	pH	Absorbance of initial MB solution	Absorbance of MB solution after adsorption	% adsorbed
1.0	20	3	1.4318	1.3210	7.74
1.0	20	7	1.3895	1.3531	2.62
1.0	20	11	1.3895	1.3112	5.64
0.5	20	7	1.3895	1.3641	1.83
1.5	20	7	1.3895	1.3587	2.22
1.0	10	7	0.6702	0.6527	2.61
1.0	30	7	2.0355	1.9409	4.65

IR spectrum of MB was attached to Figure 5 for understanding the MB adsorption capacity of BFO. As shown in Figure 5, there was no noticeable difference between IR spectrum of BFO before and after MB adsorption. Although the absorbance in the range of 500-2000 cm^{-1} slightly changed, no new absorption peaks was realized after MB adsorption. This slight change in absorbance can be argued to be due to superposition of absorption of MB, but other parts of spectrum show otherwise. The characteristic peaks of MB in the range from 2000 – 4000 cm^{-1} did

not appear in the IR spectra of 600 and 700ºC BFO samples, suggesting that the adsorption of MB on BFO samples is negligible.

Adsorbance of MB onto BFO was estimated using following fomula:

$$\text{adsorbance (\%)} = \frac{C_{thp}-C_{shp}}{C_{thp}}100\ (\%)$$

in which, C_{thp} and C_{shp} is concentration of MB after and before adsorption, respectively. The adsorbance of MB onto BFO in different pH enviroments was listed in table 1, 2.

Table 2. *Adsorbance of MB onto BFO 600°C after 60 min in dark*

BFO 600°C concentration(g/L)	MB concentration (ppm)	pH	Absorbance of initial MB	Absorbance of MB solution after adsorption	% adsorbed
1.0	20	3	1.4318	1.2556	12.28
1.0	30	7	2.0355	1.8452	9.35
1.0	20	11	1.3895	1.2442	10.46
0.5	20	7	1.3895	1.3524	2.67
1.0	20	7	1.3895	1.3531	4.12
1.5	20	7	1.3895	1.3323	3.98
1.0	10	7	0.6702	0.6433	4.01

According to table 2, a amount of adsorbed MB onto BFO 600 and 700 ºC samples was relatively small, for all investigated MB concentrations, BFO concentrations or pHs of the solution. However, BFO 600 ºC samples showed the higher MB adsorbance compared to BFO 700 ºC samples, attributed to the larger surface area (Figure 2 SEM image). Therefore, BFO powder annealed at 600 ºC is more appropriate to photocatalytic application than samples annealed at 700 ºC.

Figure 6 (a) shows the evolution of UV-Vis absorption of MB solution with illumination time. The photocatalytic degradation efficiency of MB, which was calculated via absorbance of MB solution at 640 nm, was presented in Figure 6 (b).

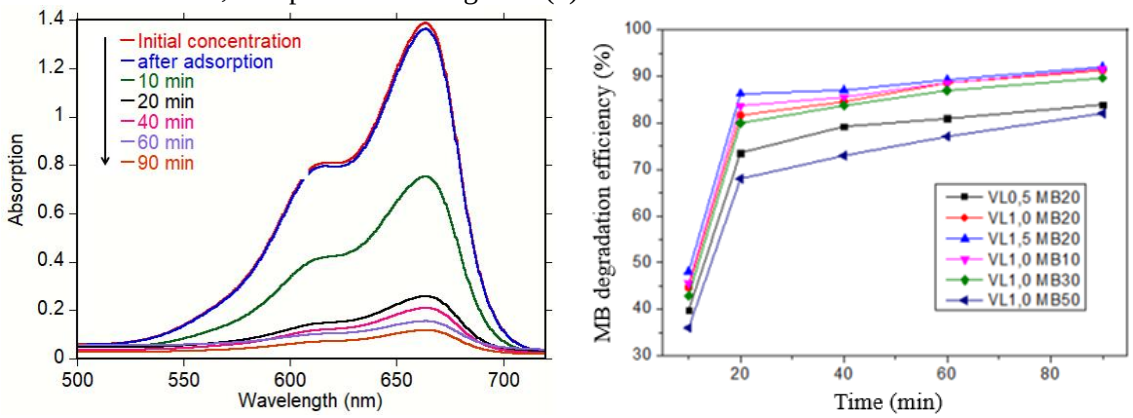

Figure 6. *(a) Evolution of absorption spectra of MB 20 ppm with solar light illumination time, under present of BFO 600 ºC powder with concentration of 1,0 g/L, and (b) Evolution of MB degradation efficiency (with various concentration of 10, 20, 30, 50 ppm) with illumination time, under the present of BFO 600 ºC powder (0,5; 1,0; 1,5 g/L)*

The results show that the degradation of MB increased drastically in the first 20 min, then increased gradually to a saturated value. When BFO concentration increased from 0.5 to 1 g/L, degradation efficiency increased from 80 % to 90% with illumination time of 90 min. However, when BFO concentration increased to 1.5 g/L, the degradation of MB was not noticeably improved compared to 1 g/L. Degradation of MB was also investigated with different MB concentrations using BFO concentration of 1g/L. There was no noticeable reduction in the MB degradation efficiency with MB concentration from 10 to 30 ppm, while it decreased from 90%

to 80% with MB concentration increased from 30 to 50ppm. According to these results, the photocatalytivity of BFO with concentration of 1 g/L showed the best efficiency in MB concentration of 30 ppm.

Dependence of MB adsorption and MB degradation efficiency on the pH of the solution were presented in Figure 7 and Figure 8 respectively. The results show that when pH of the solution changed from neutral to basic environment (pH = 11), degradation of MB almost did not change. Vice versa, when pH of the solution changed to acidic environment, pH = 3, degradation efficiency of MB decreased to only 55% in 90 min illumination. This behavior can result from the passivation of acid to BFO. Acid can dissolve part of Fe in BFO into salt, then decrease the photocatalytic activity of BFO.

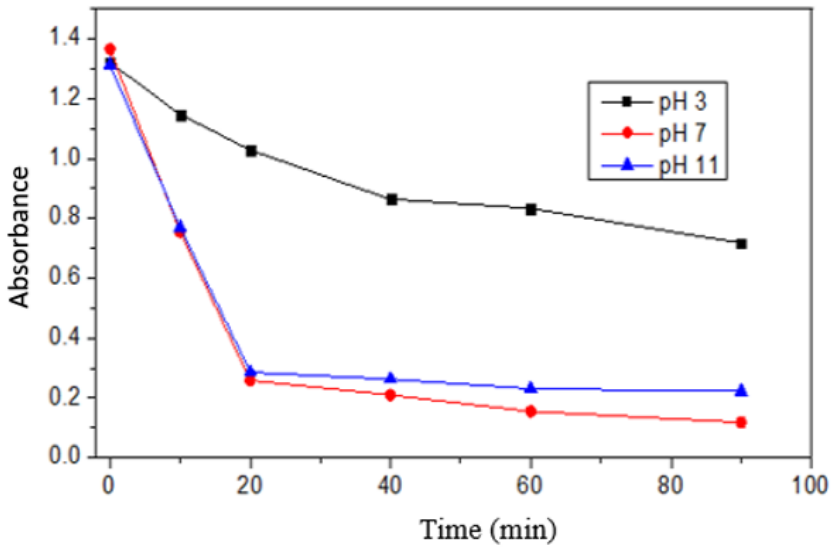

Figure 7. *Absorbance of MB 20 ppm in the solution with different pHs, under present of BFO 600 ℃, 1g/L*

Mechanism of photocatalytic reaction with present of H_2O and O_2 can be expressed as followings [27]:

$$h\nu + BFO \rightarrow h^+ + e^- \quad (1)$$

$$h^+ + \text{reactant} \rightarrow \text{product} \quad (2)$$

$$e^- + \text{reactant} \rightarrow \text{product} \quad (3)$$

$$h^+ + H_2O \rightarrow OH^* + H^+ \quad (4)$$

$$OH^* + \text{reactant} \rightarrow \text{product} \quad (5)$$

$$O_2 + e^- \rightarrow O_2^* \quad (6)$$

$$O_2^* + \text{reactant} \rightarrow \text{product} \quad (7)$$

Depending on the reagent, the degradation can occur according to reactions (2), (3), (5), (7). In general, O_2^* is quite weak so reaction (7) rarely happens. In order to determine the mechanism of photocatalyst, we studied the photocatalytic degradation of MB 20 ppm under sunlight with M1B500 1,0 g/L and with presence of t-BuOH 10 mM, $AgNO_3$ 5 mM, or $(NH_4)_2C_2O_4$ 5 mM. According to Shinde *et. al* [28], t-BuOH, $AgNO_3$, $(NH_4)_2C_2O_4$ are reagents can react with OH^*, h^+, e^-, respectively, and passivate their activity. The obtained results were shown in Figure 8.

The results show that with or without presence of t-BuOH, degradation rate did not change remarkably. With presence of $(NH_4)_2C_2O_4$, degradation rate decreased from 85 % in 20 min to 62%. With $AgNO_3$, degradation rate decreased from 85% in 20 min to 40 %. This result suggests that the loss of e^- caused the degradation of MB decreased remarkably (almost a half). The lost of h^+ also reduced the degradation rate. In opposite, the lost of OH^* did not change the degradation rate, suggesting that the photocatalytic degradation of MB were mostly occurred according to (2) and (3).

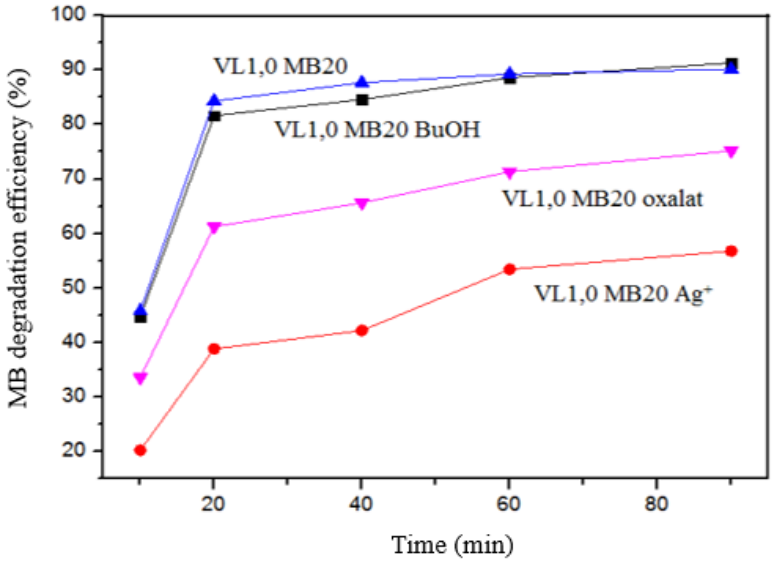

Figure 8. *Photocatalytic degradation efficiency of MB under present of BFO 600 ºC with t-BuOH, $AgNO_3$, $(NH_4)_2C_2O_4$*

4. Conclusion

We have successfully synthesized single-phase BFO materials with hollow-porous structure using sol-gel method with the complexation reagent of tartaric acid. Our BFO powder almost does not adsorb MB, but possesses excellent photocatalytic activity for MB degradation under sunlight. The degradation of MB happens quite fast in the first 20 min illumination. After 90 min illumination, degradation of MB can reach to 90% with MB 10-30 ppm solutions using a BFO dose of 1 g/L. Mechanism of MB photocatalytic degradation with BFO catalyst was shown due to reaction of e-h pairs.

Acknowledgment

This research was supported by the Ministry of Education and Training of Vietnam (B2023-TNA-09)

REFERENCES

[1] Y. Liu, Y. Wang, J. Ma, S. Li, H. Pan, and Y. Lin, "Controllable electrical, magnetoelectric and optical properties of BiFeO3 via domain engineering," *Prog. Mater. Sci.*, vol. 127, 2022, Art. no. 100943, doi: 10.1016/j.pmatsci.2022.100943.

[2] A. Haruna, I. Abdulkadir, and S. Idris, "Photocatalytic activity and doping effects of $BiFeO_3$ nanoparticles in model organic dyes," *Heliyon*, vol. 6, 2020, doi: 10.1016/j.heliyon.2020.e03237.

[3] C. Ponraj and J. Daniel, "A review on the visible light active BiFeO3 nanostructures as suitable photocatalyst in the degradation of different textile dyes," *Environ. Nanotechnol. Monit. Manag.*, vol. 7, pp. 110-120, 2017, doi: 10.1016/j.enmm.2017.02.001.

[4] R. Safi and H. Shokrollahi, "Physics, chemistry and synthesis methods of nanostructured bismuth ferrite ($BiFeO_3$) as a ferroelectro-magnetic material," *Prog. Solid. State Chem.*, vol. 40, pp. 6-15, 2012, doi: 10.1016/j.progsolidstchem.2012.03.001.

[5] P. Chen, J. Podraza, X. Xu, A. Melville, E. Vlahos, V. Gopalan, R. Ramesh, D. Schlom, and J. Musfeldt, "Optical properties of quasi-tetragonal $BiFeO_3$ thin films," *Appl. Phys. Lett.*, vol. 96, 2010, Art. no. 131907, doi: 10.1063/1.3364133.

[6] X. Xu, T. Brinzari, S. Lee, Y. Chu, L. Martin, A. Kumar, S. McGill, R. Rai, R. Ramesh, V. Gopalan, S. Cheong, and J. Musfeldt, "Optical properties and magnetochromism in multiferroic $BiFeO_3$," *Phys. Rev. B*, vol. 79, 2009, Art. no. 134425, doi:10.1103/PhysRevB.79.134425.

[7] V. Kothai and R. Ranjan "Synthesis of $BiFeO_3$ by carbonate precipitation," *Bull. Mater. Sci*, vol. 35, pp 157-161, 2012, doi: 10.1007/s12034-012-0266-x.

[8] M. Kumar, K. Yadav, and G. Varma, "Large magnetization and weak polarization in sol–gel derived $BiFeO_3$ ceramics," *Mater. Lett*, vol. 62, pp. 1159-1161, 2008, doi: 10.1016/j.matlet.2007.07.075.

[9] H. Tao, R. Zhang, R. Xiang, and J. Wu, "Lead-free rare earth-modified $BiFeO_3$ ceramics: Phase structure and electrical properties," *Mater. Des.*, vol. 120, pp. 83-89, 2017, doi: 10.1016/j.matdes.2017.01.083.

[10] Q. Yin, B. Dai, P. Zheng, J. Zhou, W. Bai, F. Wen, J. Deng, L. Zheng, J. Du, and H. Qin, "Pure-phase $BiFeO_3$ ceramics with enhanced electrical properties prepared by two-step sintering," *Ceram. Int.*, vol. 43, pp. 6467-6471, 2017, doi: 10.1016/j.ceramint.2017.02.063.

[11] M. Čebela, D. Zagorac, K. Batalović, J. Radaković, B. Stojadinović, V. Spasojević, and R. Hercigonja, "$BiFeO_3$ perovskites: A multidisciplinary approach to multiferroics," *Ceram. Int.*, vol. 43, pp. 1256-1264, 2017, doi: 10.1016/j.ceramint.2016.10.074.

[12] S. Kalikeri and V. Kodialbail, "Solar light-driven photocatalysis using mixed-phase bismuth ferrite ($BiFeO_3$/$Bi_{25}FeO_{40}$) nanoparticles for remediation of dye-contaminated water: kinetics and comparison with artificial UV and visible light-mediated photocatalysis," *Environ. Sci. Pollut. Res*, vol. 25, pp. 13881-13893, 2018, doi: 10.1007/s11356-018-1291-0.

[13] F. Majid, S. Mirza, S. Riaz, and S. Naseem, "Sol-Gel Synthesis of $BiFeO_3$, "*Nanoparticles. Mater. Today: Proc*, vol. 2, pp. 5293-5297, 2015, doi: 10.1016/j.matpr.2015.11.038.

[14] X. Wang, C. Yang, D. Zhou, Z. Wang, and M. Jin, "Chemical co-precipitation synthesis and properties of pure-phase $BiFeO_3$," *Chem. Phys. Lett.*, vol. 713, pp. 185-188, 2018, doi: 10.1016/j.cplett.2018.09.043.

[15] M. Shami, M. Awan, and M. Rehman, "Phase pure synthesis of $BiFeO_3$ nanopowders using diverse precursor via co-precipitation method," *J. Alloys Compd.*, vol. 509, pp. 10139-10144, 2011, doi: 10.1016/j.jallcom.2011.08.063.

[16] S. Pandey and S. Mishra, "Sol–gel derived organic–inorganic hybrid materials: synthesis, characterizations and applications," *J. Sol-Gel Sci. Technol.*, vol. 59, pp. 73-94, 2011, doi: 10.1007/s10971-011-2465-0.

[17] F. Gao, X. Chen, K. Yin, S. Dong, Z. Ren, F. Yuan, T. Yu, Z. Zou, and J. Liu, "Visible-Light Photocatalytic Properties of Weak Magnetic $BiFeO_3$ Nanoparticles," *Adv. Mater*, vol. 19, pp. 2889-2892, 2018, doi: 10.1002/adma.200602377.

[18] T. Gao, Z. Chen, Y. Zhu, F. Niu, Q. Huang, L. Qin, X. Sun, and Y. Huang, "Synthesis of $BiFeo_3$ nanoparticles for the visible-light induced photocatalytic property," *Mater. Res. Bull*, vol. 59, pp. 6-12, 2014, doi: 10.1016/j.materresbull.2014.06.022.

[19] S. Wang, D. Chen, F. Niu, N. Zhang, L. Qin, and Y. Huang, "Hydrogenation-induced surface oxygen vacancies in BiFeO3 nanoparticles for enhanced visible light photocatalytic performance," *J. Alloys Compd.*, vol. 688, pp. 399-406, 2016, doi: 10.1016/j.jallcom.2016.07.076.

[20] X. Wang, Y. Lin, X. Ding, and J. Jiang, "Enhanced visible-light-response photocatalytic activity of bismuth ferrite nanoparticles," *J. Alloys Compd.*, vol. 509, pp. 6585-6588, 2016, doi: 10.1016/j.jallcom.2011.03.074.

[21] S. Bharathkumar, M. Sakar, K. Rohitt, and S. Balakumar, "Versatility of electrospinning in the fabrication of fibrous mat and mesh nanostructures of bismuth ferrite ($BiFeO_3$) and their magnetic and photocatalytic activities," *Phys. Chem. Chem. Phys.*, vol. 17, pp. 17745-17754, 2015, doi: 10.1039/C5CP01640A.

[22]S. Bharathkumar, M. Sakar, and S. Balakumar, "Experimental Evidence for the Carrier Transportation Enhanced Visible Light Driven Photocatalytic Process in Bismuth Ferrite ($BiFeO_3$) One-Dimensional Fiber Nanostructures," *J. Phys. Chem. C*, vol. 120, pp. 18811-18821, 2016, doi: 10.1021/acs.jpcc.6b04344.

[23]M. Kaus, S. Imam, A. Aziz, H. Lee, R. Adnan, M. Ibrahim, and S. Yudha, "Controlled growth of $BiFeO_3$ nanoparticles in the presence of alginate template for adsorptive removal of different dyes," *Colloids Surf. A: Physicochem. Eng. Asp*, vol. 615, 2021, Art. no. 126294, doi: 10.1016/j.colsurfa.2021.126294.

[24] D. Wodka, E. Bielańska, R. Socha, M. Wodka, J. Gurgul, P. Nowak, P. Warszyński, and I. Kumakiri, "Photocatalytic Activity of Titanium Dioxide Modified by Silver Nanoparticles," *ACS Appl. Mater. Interfaces*, vol. 2, pp. 1945-1953, 2010, doi: 10.1021/am1002684.

[25] J. He, R. Guo, L. Fang, W. Dong, F. Zheng, and M. Shen, "Characterization and visible light photocatalytic mechanism of size-controlled $BiFeO_3$ nanoparticles," *Mater. Res. Bull*, vol. 48, pp. 3017-3024, 2018, doi: 10.1016/j.materresbull.2013.04.058.

[26] M. Hasan, M. Islam, R. Mahbub, M. Hossain, and M. Hakim, "A soft chemical route to the synthesis of BiFeO3 nanoparticles with enhanced magnetization," *Mater. Res. Bull*, vol. 73, pp. 179-186, 2016, doi: 10.1016/j.materresbull.2015.09.007.

[27] S. Lam, J. Quek, and J. Sin, "Mechanistic investigation of visible light responsive Ag/ZnO micro/nanoflowers for enhanced photocatalytic performance and antibacterial activity," *J. Photochem. Photobiol*, vol. 353, pp. 171-184, 2018, doi: 10.1016/j.jphotochem.2017.11.021.

[28] S. Shinde, C. Bhosale, and K. Rajpure, "Hydroxyl radical's role in the remediation of wastewater," *J. Photochem. Photobiol. B*, vol. 116, pp. 66-74, 2012, doi: 10.1016/j.jphotobiol.2012.08.003.